Monthly Notices of the ROYAL ASTRONOMICAL SOCIETY

MNRAS **512,** L21–L26 (2022) https://doi.org/10.1093/mnrasl/slac017
Advance Access publication 2022 February 22

# Evolutionary map of the Universe (EMU): 18-cm OH-maser discovery in ASKAP continuum images of the SCORPIO field

A. Ingallinera [1]★ F. Cavallaro [1,2] S. Loru,[1] J. Marvil,[3] G. Umana [1] C. Trigilio,[1] S. Breen,[4] C. Bordiu [1] C. S. Buemi,[1] F. Bufano [1] J. Collier,[2,5] S. Etoka,[6] M. D. Filipović,[5] S. R. Goldman [7] A. M. Hopkins,[8] B. S. Koribalski [5,9] P. Leto [1] R. P. Norris [5,9] S. Riggi,[1] F. Schillirò,[1] C. Tremblay [10] and J. Th. van Loon[11]

[1]*INAF - Osservatorio Astrofisico di Catania, Via Santa Sofia, 78, I-95123 Catania, Italy*
[2]*The Inter-University Institute for Data Intensive Astronomy (IDIA), Department of Astronomy, University of Cape Town, Rondebosch, Cape Town 7701, South Africa*
[3]*National Radio Astronomy Observatory, Domenici Science Operations Center, 1003 Lopezville Rd, Socorro, NM 87801, USA*
[4]*SKA Observatory, Jodrell Bank, Macclesfield SK11 9FT, UK*
[5]*School of Science, Western Sydney University, Locked Bag 1797, Penrith, NSW 2751, Australia*
[6]*JBCA, Department Physics and Astronomy, University of Manchester, Manchester M13 9PL, UK*
[7]*Space Telescope Science Institute, 3700 San Martin Drive, Baltimore, MD 21218, USA*
[8]*Australian Astronomical Optics, Macquarie University, 105 Delhi Rd, North Ryde, NSW 2113, Australia*
[9]*CSIRO Astronomy and Space Science, P.Of. Box 76, Epping, NSW 1710, Australia*
[10]*CSIRO Astronomy and Space Science, PO Box 1130, Bentley, WA 6102, Australia*
[11]*Lennard-Jones Laboratories, Keele University, Keele ST5 5BG, UK*

Accepted 2022 February 9. Received 2022 January 21; in original form 2021 October 24

## ABSTRACT

Low- and intermediate-mass stars end their life dispersing their outer layers into the circumstellar medium, during the asymptotic and post-asymptotic giant branch phases. OH masers at 18 cm offer an effective way to probe their circumstellar environment. In this work, we present the discovery of seven OH maser sources likely associated with such evolved stars from the visual inspection of Australian SKA Pathfinder (ASKAP) continuum images. These seven sources do not emit real continuum emission, but the high sensitivity of our images allows us to detect their maser emission, resembling continuum sources. To confirm their nature, we carried out spectral-line observations with ATCA. All the sources showed the double-peaked spectra at 1612 MHz, typical of evolved stars. The detection of maser emission in continuum images can be a complementary and easy-to-use method to discover new maser sources with the large-area deep surveys conducted with the Square Kilometre Array (SKA) precursors. The implication for radio stars studies are remarkable since pure OH maser sources (i.e. with no continuum associated) represent, at a sensitivity of 100 μJy beam$^{-1}$, about 4 per cent of all Galactic sources and by far the most numerous stellar population.

**Key words:** masers – methods: observational – techniques: image processing – stars: AGB and post-AGB – circumstellar matter – radio lines: stars.

## 1 INTRODUCTION

At the end of their life, low- and intermediate-mass stars ($\lesssim 8 M_\odot$ at the beginning of the main sequence) evolve from the asymptotic giant branch (AGB), when they shed their outer layers forming a circumstellar envelope (CSE), towards the planetary nebula (PN) phase (Habing 1996). The material in the CSE can condense to form dust, which absorbs the radiation from the central star and re-emits the absorbed light in the infrared (IR). The AGB phase ends when most of the outer layers have been shed. Then, the net mass-loss rate decreases and the star enters the post-AGB stage, the intermediate phase between AGB stars and PNe (van Winckel 2003). The resulting dust and gas nebula surrounding the post-AGB stars is usually referred to as the proto-planetary nebula (PPN). At the end of this process, the central inner layers are hot enough to ionize the CSE and the star enters the PN phase.

Post-AGB stars, PPNe, and young PNe are still poorly studied objects. However, during these transitions, many phenomena are believed to take place, which are responsible for the physical properties of the resultant PN. In particular: the CSE may become strongly asymmetric with respect to an initially roundish AGB envelopes (Sahai & Trauger 1998; Ragland et al. 2008); the radio continuum, if detected, can show a non-thermal synchrotron-like behaviour, lost in the final PN (thermal emitters) (Cerrigone et al. 2017); the PN may fail to emerge at all (Gesicki, Zijlstra & Miller Bertolami 2018). It is plausible that these transitional phenomena begin at the very end of the AGB stage, when O-rich AGB stars undergo the so-called OH/IR phase. The AGB stars are not expected to have a detectable radio continuum emission; however, in their CSE, as well

★ E-mail: adriano.ingallinera@inaf.it

as in those surrounding post-AGB stars and young PNe, conditions for maser emission from different molecules occur (Goldreich & Scoville 1976). Masers of OH, SiO, and $H_2O$ are common from these CSEs. The four OH 18-cm lines arise from its ground state ($^2\Pi_{3/2}$, $J = 3/2$), split by $\Lambda$-doubling and hyperfine interaction into four sub-levels (e.g. Elitzur 1992). The rest frequencies are approximately 1612, 1665, 1667, and 1720 MHz. The first three of them characterize most of the duration of the aforementioned phases, while the last is not expected in these stars (apart from exceptional cases, e.g. Sevenster & Chapman 2001). Since OH masers can form only under very peculiar condition of the CSE in terms of chemical abundances, expansion velocity field, and density, they are a perfect probe to investigate the chemical and mechanical properties of stellar ejecta (Elitzur 1992).

The search for new masers is therefore a fundamental step toward a deeper understanding of the evolutionary process of an AGB star towards the PN phase. An unexpected aid to this quest is coming from the deep, large-area surveys conducted with the Square Kilometre Array (SKA) precursors. In particular, within the Evolutionary Map of the Universe (EMU; Norris et al. 2011, 2021) survey programme, the Australian SKA Pathfinder (ASKAP; Hotan et al. 2021; Johnston et al. 2008) is observing the entire southern sky ($\delta < +30^\circ$) at a central frequency of $\sim$1.2 GHz. During the early science phase and in preparation for EMU, ASKAP observed the Galactic 'SCORPIO' field (Umana et al. 2015, 2021) between 2018 and 2019, in all its three bands, with a frequency range spanning from 0.7 to 1.7 GHz. In this paper, we describe how we used these EMU/ASKAP continuum observations to discover new OH-maser sources and the follow-up observations we carried out to confirm their nature. The final aims are to expose a new general method applicable to deep, large-area continuum surveys to search for new maser sources and quantify their contribution to Galactic continuum point-source catalogues. In Section 2, we describe the EMU/ASKAP observations and the methodologies we employed to discover and support the new detections. In Section 3, we describe the follow-up ATCA observations for the confirmation of their maser-emitting AGB or post-AGB nature. A discussion is presented in Section 4 and summary and conclusions in Section 5.

## 2 ASKAP OBSERVATIONS AND SOURCE DETECTION

### 2.1 ASKAP observations

The SCORPIO field (Umana et al. 2015, 2021) was observed with the ASKAP full array (30 antennas over 36 working) in band 1 (central frequency 900 MHz), 2 (1250 MHz), and 3 (1550 MHz) in 2019 (scheduling blocks SB8838, SB8845, and SB8850), within the preparatory work for the EMU survey. The observation provided an almost continuous frequency coverage from 0.75 to 1.7 GHz (net bandwidth 864 MHz). The total integration time was 33 h, 11 h per band. The chosen beam configuration was 'square 6x6', consisting of a regular square grid and a total number of 36 phased array beams (Schinckel & Bock 2016) in a single footprint (no interleaving).

The first part of the data reduction was performed by the ASKAP data reduction team on the Galaxy supercomputer at the Pawsey Computing Centre. The data were calibrated for bandpass and absolute flux density by observing the standard calibrator PKS 1934–638, using the ASKAPSOFT pipeline (Guzman et al. 2019; Wieringa, Raja & Ord 2020). Within this pipeline, the data were subsequently automatically flagged, channel-averaged, and flagged again. The averaging process reduced the number of channels from 16 384 per band to 288 (channel width 1 MHz). We imaged and self-calibrated the data with CASA and WSCLEAN (McMullin et al. 2007; Offringa et al. 2014), using all the three data sets (one per band) as an input and creating in output five different maps, hereafter the 'sub-band maps', each one 145-MHz (sub-band 1, 2 and 5) or 125-MHz (sub-band 3 and 4) wide.

Once all the 36 beams were linearly mosaiced, the five maps covered a sky region ranging from $\sim$30 to $\sim$40 deg$^2$, depending on the central frequencies. The restoring beam was forced to be $14 \times 14$ arcsec$^2$ (approximately the PSF size at the lowest frequency) and the maps are pixel-to-pixel coincident (pixel size 1.5 arcsec). These data suffer from a poor primary beam correction since the ASKAP primary beam was not accurately measured for these observations. While this greatly affects the general analysis of these images (above all the inaccuracy of flux densities), it has a negligible effect in our analysis, since we use these images only for the purpose of detecting sources.

### 2.2 Detecting maser-emitting sources in continuum maps

The original rationale of having five sub-band maps was to easily allow a spectral characterization of the sources, thanks to the large ASKAP fractional bandwidth ($\sim$0.7). The production of sub-band images is an easy and effective procedure when observing with large bandwidth in pseudo-continuum mode (i.e. using a large number of spectral channels, eventually averaged to produce a final map; e.g. Hurley-Walker et al. 2019).

A first visual inspection of these maps showed that at least 24 sources were detected only in the fifth map. An extensive search in published catalogues and a closer look at these sources showed that all of them were associated with known OH maser sources: the line emission was 'diluted' in the wide band, but still detectable.

To show even more clearly the OH-maser nature of these sources, we created three other maps with CASA using only one single 1-MHz channel from the averaged calibrated visibilities, namely channels centred at 1610.9, 1611.9, and 1612.9 MHz. The LSR velocity range covered is from $-220$ to 340 km s$^{-1}$, while the expected velocities for this line of sight range from $-160$ to 30 km s$^{-1}$. In these 1-MHz maps, the synthesized beam was left equal to the main lobe of the point spread function, varying negligibly around a typical value of $15 \times 10$ arcsec$^2$.

After the inspection of the 1-MHz maps, a total of 49 sources were tagged as potential OH-maser sources as appearing only in the fifth sub-band image and only in one 1-MHz map. Among these, 42 were associated with known OH-maser sources (25 classified as evolved stars, one star-forming region, and 16 unclassified, the complete list is in Section A), while the other seven were not found in any catalogue reported in the VizieR data base,[1] with a search radius of 2 arcmin. A subsequent search in the `maserdb.net` data base did not return any OH-maser associations either, though one source (G341.2969+0.3504) is associated with an $H_2O$ maser within 1 arcsec. Nonetheless, we suspected that these seven sources were also truly OH-maser sources associated with AGB stars. Such a discovery would impact radio star studies in continuum emission, where OH masers from AGB stars would act as contaminants in star samples. It would also open up a possible use of future continuum surveys for a purpose far from their design goals. Thus, we decided to investigate further our speculation regarding the nature of these seven unclassified sources. We first searched for an IR counterpart

[1] https://vizier.u-strasbg.fr/viz-bin/VizieR

(Section 2.3), and we then conducted radio spectral-line observations on all of them (Section 3). The other 51 known OH maser sources fall within our field of view but are not detected in our images, possibly because of variability or intensity issues (see also Section 4).

### 2.3 Cross-matching IR stars

A comparison with images from the GLIMPSE survey conducted with the *Spitzer Space Telescope* (Benjamin et al. 2003; Churchwell et al. 2009) showed that our seven OH-maser candidates are within 4 arcsec of stars with IR colours redder than their neighbours (thus excluding the effect of local extinction), compatible with IR excess. The astrometric accuracy of GLIMPSE[2] and ASKAP (Riggi et al. 2021) are better than 2 arcsec. Consequently, the separation between an ASKAP radio source and the corresponding (GLIMPSE) IR counterpart can be used straightforwardly for cross-matching. We computed the colour of each source as the difference between the magnitudes at 3.6 μm and at 5.8 μm from the GLIMPSE point source catalogue and the average colour of all the stars within 30 arcsec for which these magnitudes were available. This choice of colours maximized the number of neighbour stars with photometric measurements (from 9 to 16). In Table 1, we report these results.

The GLIMPSE survey is confused, and the possibility that our matches are spurious is not negligible. Using the method described in Umana et al. (2015), we cross-matched the GLIMPSE catalogue with 14 fictitious positions obtained by shifting our maser locations by 1 arcmin north and south. In three cases, no star was detected within 4 arcsec. The remaining 11 detected in these false positions do not show characteristics expected for evolved stars: they are all faint ([3.6] $>$ 13 mag) and only one has a measurement in the 5.8-μm band (and its [3.6] $-$ [5.8] colour is 0.5 mag). Based on these considerations, we do not believe that our matches are spurious.

For the targeted sources, the errors reported in Table 1 are computed by propagation of the errors supplied by the catalogue. For the other stars, the spread provided is the standard deviation of the sample. All the sources have redder colours than the average of their neighbours, the first four with a high statistical significance. This result supports the possibility that our maser candidates are associated with AGB or post-AGB stars, though only the IR source GLIMPSE G341.2967+00.3491 is classified in the literature as such (Robitaille et al. 2008).

## 3 SPECTRAL-LINE FOLLOW-UPS

### 3.1 ATCA observations

ATCA spectral line observations of the seven new OH maser candidates were conducted in June 2021, with the array in the 6B configuration (project C3414). The CABB backend was set up to the CFB 1M-0.5k mode, with a spectral resolution of 0.5 kHz (Wilson et al. 2011). The total observing time was 12 h. The standard source PKS 1934–638 was observed as a flux calibrator.

The data reduction was carried out using CASA. Calibration for gain and flux density was performed using the tasks GAINCAL and FLUXSCALE. For each source, a data cube was produced, centred on the source. The original channels were re-binned to 3-kHz channels, still sufficiently narrow to well sample the typical OH-maser features of AGB and post-AGB stars (Ingallinera et al. 2015). The image dimensions were set to 128 $\times$ 128 pixel, with each pixel 1-arcsec wide and the synthesis beam about 11.4 $\times$ 7.8 arcsec$^2$.

### 3.2 Analysis of the spectra

We used the data cubes produced in Section 3.1 to extract four spectra for each source, that is one for each of the four ground-state OH-maser transitions. The spectra were extracted in a region comprising the synthesized beam centred on the map centre with the 'Spectral Profile Tool' in CASA. At 1720 MHz, no lines were detected, and this frequency will not be further considered in this work. The spectra at 1612, 1665, and 1667 MHz, grouped per source, are shown in Appendix B (available as supplementary material), a preview is presented in Fig. 1.

At 1612 MHz, all the spectra show the classical profile of an expanding shell, usually associated with AGB stars. In Table 2, we report the velocities and the flux densities of the two peaks, indicated by the index 1 or 2. The velocity separation of the two peaks, whose half-value is a measure of the shell expansion velocity at a distance of $\sim$0.003 pc from the star, is in the typical range for AGB stars (10–25 km s$^{-1}$ rather than that of red supergiant stars; see for example Engels & Bunzel 2015; Goldman et al. 2017). The main lines (1665 and 1667 MHz) are detected only for G342.6443+0.1142. They are both single-peaked and their velocity is close to the mid-point of the 1612-MHz peaks, compatible with their formation in the inner parts of the nebula. Indeed, for this source, the 1612-MHz spectrum shows quite broad lines, with respect to the others, and the determination of the exact mid-point is not easy.

The error associated with the flux densities reported in Table 2 is the standard deviation of the spectrum in a spectral region devoid of emission and well outside the velocity range of the detected lines. It does not take into account the absolute flux density error. All the lines are detected with a significance of at least $\sim 5\sigma$, with the only exception of one 1612-MHz line of G342.6443+0.1142 ($4\sigma$). Since artefacts from distant maser sources may give a false positive in our spectra, in the Appendix B we also show the images of each source at the velocity of both the peaks of the 1612-MHz line and, for G342.6443+0.1142, at the peaks of the main lines. From these images, the association of all our spectra with the targeted sources is clear.

Other Galactic sources like star-forming regions may present OH masers, usually more prominent at 1665 and 1667 MHz. However, these sources are usually characterized also by a continuum emission, which is not detected in our cases, and a different behaviour at 1612 MHz. Given this lack of continuum emission, the 1612-MHz line shapes and the IR counterparts, we conclude that our seven sources are almost certainly AGB or post-AGB stars.

## 4 DISCUSSION

The OH maser emission is an important probe for the environment of AGB and post-AGB stars since it is directly linked to their circumstellar envelope density and expansion velocity.

The advent of the SKA precursors provides new possibilities for maser surveys. For example, the spectral-line 'Galactic ASKAP survey' (GASKAP) will supply data with unprecedented sensitivity (Dickey et al. 2013). Continuum all-sky surveys can be a complementary tool to extend the sky coverage of spectral-line surveys, limited by sensitivity requirements. EMU is going to observe the entire southern sky, including the Galactic plane without Galactic latitude constraints. Its sensitivity is designed to be around 15 μJy beam$^{-1}$, much less than any other current all-sky survey at these frequencies.

[2] http://www.astro.wisc.edu/glimpse/GQA-master.pdf

**Table 1.** IR counterparts of the ASKAP maser sources. The first three columns list the conventional name we gave to the sources in our sample and their radio coordinates; the fourth column lists cross-matched GLIMPSE sources. The fifth and sixth columns report the target and stellar neighbourhood colours ([3.6] − [5.8]) as explained in the text. In the last column, we list the separation between our radio source and the corresponding IR counterpart.

| ASKAP source | Right ascension (J2000) | Declination (J2000) | GLIMPSE name [GLIMPSE] | Target colour | Average colour | Distance (arcsec) |
|---|---|---|---|---|---|---|
| G341.2969+0.3504 | $16^h50^m09\overset{s}{.}7$ | $-44°01'42''$ | G341.2967+00.3491 | $2.9 \pm 0.1$ | $0.6 \pm 0.5$ | 4.0 |
| G341.3970+0.0159 | $16^h51^m57\overset{s}{.}1$ | $-44°09'53''$ | G341.3971+00.0153 | $1.4 \pm 0.1$ | $1.3 \pm 1.3$ | 2.1 |
| G342.6443+0.1142 | $16^h55^m53\overset{s}{.}0$ | $-43°08'07''$ | G342.6441+00.1136 | $2.1 \pm 0.1$ | $1.5 \pm 0.8$ | 1.7 |
| G343.2533−0.0749 | $16^h58^m46\overset{s}{.}0$ | $-42°46'37''$ | G343.2535-00.0755 | $2.1 \pm 0.1$ | $0.4 \pm 0.3$ | 2.2 |
| G343.3031−0.8634 | $17^h02^m19\overset{s}{.}9$ | $-43°13'24''$ | G343.3030-00.8635 | $2.0 \pm 0.1$ | $0.6 \pm 0.6$ | 0.8 |
| G343.9724−0.1879 | $17^h01^m39\overset{s}{.}4$ | $-42°16'50''$ | G343.9723-00.1883 | $2.7 \pm 0.1$ | $0.5 \pm 0.3$ | 1.2 |
| G344.2963+0.1540 | $17^h01^m16\overset{s}{.}4$ | $-41°48'54''$ | G344.2959+00.1542 | $1.7 \pm 0.1$ | $1.5 \pm 1.5$ | 1.6 |

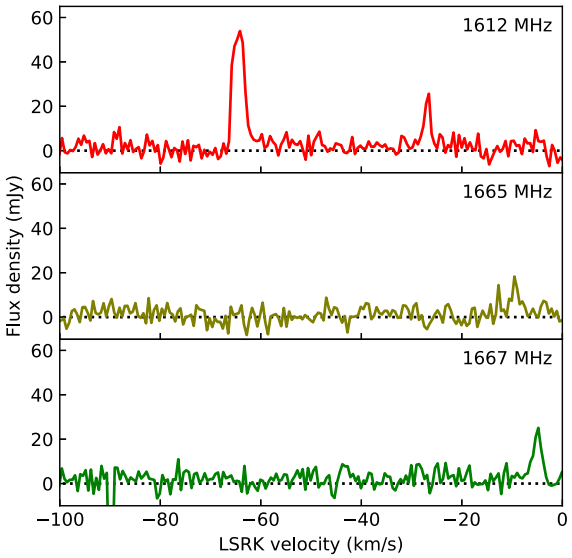


**Figure 1.** Spectrum of G341.2969+0.3504.

Besides observing the Galactic plane, EMU will also allow us to probe Galactic latitude higher than $\pm 1°$. The observing and reduction strategy described in Section 2 can be adopted without any particular observing requirement. The availability of channel-averaged, calibrated visibilities, such as those in Section 2, and their imaging, is not even necessary once the method here has shown its robustness and new surveys have gone deeper in sensitivity. We acknowledge that continuum images cannot be used to fully characterize new maser sources, since they only supply information on their position. However, as demonstrated here, they can be used for an initial blind search, as a base for targeted spectral-line observations.

All-sky continuum surveys have the potential to discover new maser sources far from the Galactic plane, in regions normally not included in Galactic surveys. Furthermore, our method can also be applied to red-shifted extragalactic OH megamasers (Staveley-Smith et al. 1992), especially if the EMU frequency coverage is not going to include the OH rest frequency (the actual frequency range of EMU is still to be defined). In this case, continuum images from EMU would complement the spectral-line observations of the WALLABY ASKAP survey (Koribalski et al. 2020).

It is difficult to predict how bright an OH-maser source is in continuum images. As a raw estimate, one can integrate the flux density from the spectrum over a frequency range encompassing all the lines and then scale this integrated flux density by the bandwidth of the continuum map. For example, integrating G343.9724−0.1879 over a range of 300 kHz including all the line emission, we obtain a total flux density of 121.5 kJy Hz, which would appear as a source of about 800 μJy in a 145-MHz wide image or ∼100 mJy in a 1-MHz map. It has to be noted that this computation does not take into account at least two major complications: some channels have been flagged, and the imaging process may introduce further non-linear smoothing of sharp spectral features during a multifrequency synthesis. These effects may create some discrepancy on the expected value.

For the same reason, it is extremely difficult to derive quantitative information of the lines from continuum images. When we wrote the proposal for the ATCA follow-up, we used eight known maser sources visible in our ASKAP data to check if a relation existed between their continuum flux density and the corresponding line intensity. We found that the mean ratio between the line intensity and the source flux density was around 115 (hereafter the 'calibration factor'), but with a huge spread of values, ranging from 45 to 210. We set our requested observing time in order to have a mean signal-to-noise ratio of 10 for all the sources with the native 0.5-kHz channels. After rebinning to 3 kHz we would expect a possible increase in the signal-to-noise ratio of a factor $\lesssim \sqrt{6}$. Indeed, looking at Table 2, we can see that the actual signal-to-noise ratio, calculated as the ratio between the peak flux density and its error, is close to what is expected. The possibility to estimate the intensity of the OH-maser sources in continuum images, at least to an order of magnitude, is relevant in order to have an idea of what impact future continuum surveys with next-generation instruments, like SKA, may have. The presence of maser sources in continuum images may play an important role for Galactic radio astronomy and in particular for the study of radio stars. In our ASKAP field (rms $\sim 100\,\mu\mathrm{Jy\,beam^{-1}}$), OH-maser sources associated with AGB or post-AGB stars represent more than 1 per cent of all the point sources extracted (3963; Riggi et al. 2021), around 4 per cent of all the estimated Galactic sources (estimated as roughly 1/4 of the total sources) and, by far, the most numerous stellar population (20 stars with a continuum emission have been identified so far in this field; Riggi et al. 2021). Stellar studies that will rely on the analysis of surveys like EMU should take into account that a relevant fraction of point-like Galactic sources will be of the type presented in this work.

## 5 SUMMARY AND CONCLUSIONS

We used ASKAP continuum images to detect and discover OH maser emission from AGB stars. These sources are not expected to show radio continuum emission, but the sensitivity reached in our

**Table 2.** Line velocities and flux densities. For 1612-MHz lines, $v_1$ and $v_2$ are the velocities of the two peaks at 1612 MHz, $\Delta v/2$ is the semi-difference between these two values (i.e. the expansion velocity of the CSE) and $S_1$ and $S_2$ the corresponding flux densities. For the 1665 and 1667 MHz only one velocity and flux density value is reported since these are single-peaked lines. The last two columns report the nearer and farther kinematic distances derived from the Galactic rotation model.

| Source name | Line (MHz) | $v_1$ (km s$^{-1}$) | $v_2$ (km s$^{-1}$) | $\Delta v/2$ (km s$^{-1}$) | $S_1$ (mJy) | $S_2$ (mJy) | Distances near (kpc) | far (kpc) |
|---|---|---|---|---|---|---|---|---|
| G341.2969+0.3504 | 1612 | 0.1 | 24.1 | 12.0 | 58 ± 5 | 98 ± 5 | - | 17.2 |
| G341.3970+0.0159 | 1612 | − 69.6 | − 31.5 | 19.0 | 30 ± 4 | 70 ± 4 | 3.8 | 12.2 |
| G342.6443+0.1142 | 1612 | − 99.0 | − 48.9 | 25.1 | 47 ± 9 | 36 ± 9 | 4.8 | 11.2 |
| G342.6443+0.1142 | 1665 | − 71.8 | - | - | 44 ± 9 | - | | |
| G342.6443+0.1142 | 1667 | − 63.8 | - | - | 46 ± 9 | - | | |
| G343.2533−0.0749 | 1612 | − 124.1 | − 102.8 | 10.6 | 50 ± 5 | 67 ± 5 | 6.0 | 10.0 |
| G343.3031−0.8634 | 1612 | − 87.6 | − 58.7 | 14.4 | 33 ± 4 | 45 ± 4 | 4.8 | 11.3 |
| G343.9724−0.1879 | 1612 | − 64.1 | − 26.6 | 18.8 | 54 ± 3 | 27 ± 3 | 3.7 | 12.4 |
| G344.2963+0.1540 | 1612 | − 33.6 | 14.8 | 24.2 | 70 ± 8 | 78 ± 8 | 1.3 | 14.9 |

observations is high enough that the narrow-line emission is still detectable even in wide-band images. Our method produces sub-band images, useful for spectral analysis, to detect sources visible only in the sub-band where the maser emission occurs. Targeted follow-up spectral-line observations validated the maser nature of these unusual sources. Although no quantitative information can be extracted from continuum images, the possibility to detect and precisely locate new maser source candidates can be a starting point for follow-up characterization through deeper targeted observations. From the point of view of Galactic radio astronomy, the identification of these sources and their classification as low- and intermediate-mass evolved stars have a great impact in radio star studies at this frequency since we have shown that the total number of pure maser sources in continuum images is not negligible, and will increase once higher sensitivity images become available.

## ACKNOWLEDGEMENTS

The Australian SKA Pathfinder is part of the Australia Telescope National Facility, which is managed by CSIRO. Operation of ASKAP is funded by the Australian Government with support from the National Collaborative Research Infrastructure Strategy. The establishment of the Murchison Radio-astronomy Observatory was funded by the Australian Government and the Government of Western Australia. This work was supported by resources provided by the Pawsey Supercomputing Centre with funding from the Australian Government and the Government of Western Australia. We acknowledge the Wajarri Yamatji people as the traditional owners of the Observatory site. This research has made use of the VizieR catalogue access tool, CDS, Strasbourg, France.

## DATA AVAILABILITY

The data cubes and the spectra used in this work are publicly available at https://doi.org/10.5281/zenodo.5865531. A table listing all previously known maser sources in the field is reported in Appendix A as supplementary material.

## REFERENCES

Benjamin R. A. et al., 2003, PASP, 115, 953
Cerrigone L., Umana G., Trigilio C., Leto P., Buemi C. S., Ingallinera A., 2017, MNRAS, 468, 3450
Churchwell E. et al., 2009, PASP, 121, 213
Dickey J. M. et al., 2013, Publ. Astron. Soc. Aust., 30, 3
Elitzur M., 1992, Astronomical Masers, Kluwer, Dordrecht,
Engels D., Bunzel F., 2015, A&A, 582, A68
Gesicki K., Zijlstra A. A., Miller Bertolami M. M., 2018, Nat. Astron., 2, 580
Goldman S. R. et al., 2017, MNRAS, 465, 403
Goldreich P., Scoville N., 1976, ApJ, 205, 144
Guzman J. et al., 2019, ASKAPsoft: ASKAP science data processor software. preprint (ascl:1912.003)
Habing H. J., 1996, A&ARv, 7, 97
Hotan A. W. et al., 2021, Publ. Astron. Soc. Aust., 38, 9
Hurley-Walker N. et al., 2019, Publ. Astron. Soc. Aust., 36, 47
Ingallinera A., Trigilio C., Leto P., Umana G., Buemi C., Cerrigone L., Agliozzo C., 2015, MNRAS, 453, 3203
Johnston S. et al., 2008, Exp.Astron., 22, 151
Koribalski B. S. et al., 2020, Ap&SS, 365, 118
McMullin J. P., Waters B., Schiebel D., Young W., Golap K., 2007, in Shaw R. A., Hill F., Bell D. J., eds, ASP Conf. Ser. Vol. 376, Astronomical Data Analysis Software and Systems XVI. p. 127
Norris R. P. et al., 2011, Publ. Astron. Soc. Aust., 28, 215
Norris R. P. et al., 2021, PASA, 38, 46
Offringa A. R. et al., 2014, MNRAS, 444, 606
Qiao H.-H. et al., 2016, ApJS, 227, 26
Ragland S. et al., 2008, ApJ, 679, 746
Riggi S. et al., 2021, MNRAS, 502, 60
Robitaille T. P. et al., 2008, AJ, 136, 2413
Sahai R., Trauger J. T., 1998, AJ, 116, 1357
Schinckel A. E. T., Bock D. C. J., 2016, in Hall H. J., Gilmozzi R., Marshall H. K., eds, SPIE Conf. Ser. Vol. 9906, Ground-based and Airborne Telescopes VI. p. 99062A
Sevenster M. N., Chapman J. M., 2001, ApJ, 546, L119
Staveley-Smith L., Norris R. P., Chapman J. M., Allen D. A., Whiteoak J. B., Roy A. L., 1992, MNRAS, 258, 725
Umana G. et al., 2015, MNRAS, 454, 902
Umana G. et al., 2021, MNRAS, 506, 2232
van Winckel H., 2003, A&ARv, 41, 391
Wieringa M., Raja W., Ord S., 2020, in Pizzo R., Deul E. R., Mol J. D., de Plaa J., Verkouter H., eds, ASP Conf. Ser. Vol. 527, Astronomical Data Analysis Software and Systems XXIX. p. 591
Wilson W. E. et al., 2011, MNRAS, 416, 832

## SUPPORTING INFORMATION

Supplementary data are available at *MNRASL* online.

**Table A1.** A complete list of all known maser sources detected in our images from the catalogues by Engels & Bunzel (2015) and Qiao et al. (2016), reported as 'E' and 'Q' in the reference column.
**Figure B1.** Spectra of G341.2969+0.3504.
**Figure B2.** Peak images of G341.2969+0.3504.

**Figure B3.** Spectra of G341.3970+0.0159.
**Figure B4.** Peak images of G341.3970+0.0159.
**Figure B5.** Spectra of G343.2533−0.0749.
**Figure B6.** Peak images of G343.2533−0.0749.
**Figure B7.** Spectra of G343.3031−0.8634.
**Figure B8.** Peak images of G343.3031−0.8634.
**Figure B9.** Spectra of G343.9724−0.1879.
**Figure B10.** Peak images of G343.9724−0.1879.
**Figure B11.** Spectra of G344.2963+0.1540.
**Figure B12.** Peak images of G344.2963+0.1540.
**Figure B13.** Spectra of G342.6443+0.1142.
**Figure B14.** Peak images of G342.6443+0.1142 relative to the 1612-MHz data cube.
**Figure B15.** Peak images of G342.6443+0.1142 relative to the 1665 and 1667-MHz data cubes.



This paper has been typeset from a TEX/LATEX file prepared by the author.